Food Chemistry 514 (2026) 148970

Contents lists available at ScienceDirect

Food Chemistry

journal homepage: www.elsevier.com/locate/foodchem

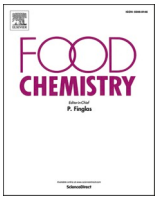

Investigating the crystalline structure and structural heterogeneity of starch granules using polarization-based quantitative phase microscopy

Samira Ebrahimi [a,b,1], Yu Tian [c,1], Andreas Blennow [a], Ke Guo [f], Sheng Chen [d], Liselotte Jauffred [b,h], Poul Martin Bendix [b], Jacob Judas Kain Kirkensgaard [b,g], Staffan Persson [a,e,*], Yuyue Zhong [d,**]

[a] Department of Plant and Environmental Sciences, Copenhagen Plant Science Center (CPSC), University of Copenhagen, Denmark
[b] Niels Bohr Institute, University of Copenhagen, Copenhagen, Denmark
[c] Lab of Food Soft Matter Structure and Advanced Manufacturing, College of Food Science and Engineering, Collaborative Innovation Center for Modern Grain Circulation and Safety, Nanjing University of Finance and Economics, Nanjing 210023, China
[d] Department of Food Science and Nutrition, The Hong Kong Polytechnic University, Hung Hom, Kowloon, Hong Kong, China
[e] Joint International Research Laboratory of Metabolic and Developmental Sciences, State Key Laboratory of Hybrid Rice, School of Life Sciences and Biotechnology, Shanghai Jiao Tong University, Shanghai, China
[f] Institute of Food Crops, Jiangsu Academy of Agricultural Sciences, Nanjing 210014, China
[g] Department of Food Science, University of Copenhagen, DK-1958 Frederiksberg C, Denmark
[h] DTU Bioengeenering, Technical University of Denmark, 2800 Kgs. Lyngby, Denmark

ARTICLE INFO

Keywords:
Maltese cross
Birefringence
Digestion
Amylose
Digital holographic microscopy

ABSTRACT

A thorough understanding of starch structure from crystal distribution level is crucial for production, processing, and application of starch. In this study, we utilized a custom-built polarization-based quantitative phase microscopy based on digital holography as well as a multimodal polarization microscope to investigate the crystalline structure of starch granules at the level of the Maltese cross. Through quantitative analysis, we observed that crystalline regions are distributed on both sides of the granules, with non-crystalline material extending radially in between, with amylose playing a significant role in disrupting this crystal alignment. This offers insights into why starch granules exhibit low overall crystallinity, often below 20%, as observed in maize and potato starches. Additionally, in situ enzymatic hydrolysis and digestion analysis of starch granules revealed the rapid breakdown of granular structures at specific points in the process. The crystalline heterogeneity, quantified as variation in birefringence intensity (with standard deviations of 25–50% for maize starch and 13–25% for potato starch), which was observed across the granule population of the same starch type, resulted in asynchronous granule disruption, emphasizing the structural complexity within starch granules. These findings contribute to a deeper understanding of current models of starch structure, particularly in terms of how crystalline and amorphous regions interact during gelatinization and enzymatic processes. This study offers deeper insights into starch structure-function relationships and underscores the value of digital holographic quantitative phase microscopy for starch analysis.

1. Introduction

Starch accounts for 70%–80% of the calories consumed globally and is a key component in many foods due to its desirable functional and nutritional properties, which are important to e.g. the food industries (Muñoz, Pedreschi, Leiva, & Aguilera, 2015). Starch is biosynthesized as

Abbreviations: BF, bright field; DIC, differential interference contrast; DHM, digital holographic microscopy; GLIM, gradient light interference microscopy; HMS, high amylose maize starch; HPS, high amylose potato starch; NMS, normal maize starch; NPS, normal potato starch; PM, polarized Microscopy; QPM, quantitative phase microscopy; SEC, size exclusion chromatography; WMS, waxy maize starch; WPS, waxy potato starch; WAXS, wide angle X-ray scattering.

* Corresponding author at: Department of Plant and Environmental Sciences, Copenhagen Plant Science Center (CPSC), University of Copenhagen, Denmark.
** Corresponding author.
E-mail addresses: staffan.persson@plen.ku.dk (S. Persson), yuyuezhong93@163.com (Y. Zhong).
[1] These authors contributed equally to this work.

https://doi.org/10.1016/j.foodchem.2026.148970
Received 12 September 2025; Received in revised form 14 February 2026; Accepted 19 March 2026
Available online 27 March 2026

semicrystalline granules with a hierarchical and multiscale organization, featuring structural elements ranging from glucose monomers at the nanometer scale to granules of several micrometers (Lourdin et al., 2015). The granules comprise crystalline and amorphous lamellae with a repeat distance of 9–10 nm, blocklets measuring 30–200 nm, growth rings ranging from 200 to 600 nm, and other supramolecular arrangements such as superhelices (Lourdin et al., 2015). This multi-level starch structure determines its functionality and applications. Research on structural features of starch is therefore important to both academic and applied science.

As well known, the disappearance of the Maltese cross, which indicates the orderly alignment of amylose and amylopectin molecules within the granules, is a key indicator of structural changes in starch granules and is characteristic to starch hydrothermal hydration and disassembly, a process known as gelatinization (Cai & Wei, 2013; Cai, Zhao, Huang, Chen, & Wei, 2014; Liu, Charlet, Yelle, & Arul, 2002; Patel & Seetharaman, 2006; Yeh & Li, 1996) and digestion (Ding et al., 2021; Fuwa, Sugimoto, Takaya, & Nikuni, 1979). A deeper understanding of starch granule birefringence for different types of starch granules depending on e.g. its content of amylose may provide valuable insights into the architecture and functionality of starch granules.

The Maltese cross pattern in starch granules is observed using polarized microscopy, a technique that exploits the concept of polarization, which describes the direction of oscillation of electromagnetic radiation. Polarization measurements can assess the molecular-level birefringence of optically anisotropic materials which have two different refractive indices and refract the incoming light into two rays due to the ordered arrangement of their internal microstructures. Polarized microscopy, specifically, measures phase retardation and optical axis orientation in transparent specimens by acquiring multiple images with different polarization configurations (Bunker & Anderson, 1928; Xiao et al., 2020).

Polarization microscopy methods such as differential interference contrast (DIC) microscopy have traditionally been associated with qualitative imaging of anisotropic materials (Xiao et al., 2020). The first quantitative birefringence analyses were done by sequential acquisition at different phase retardance delays (Abraham & Elbaum, 2013; Mehta, Shribak, & Oldenbourg, 2013). This time-consuming approach limits its ability to measure dynamic processes that impact birefringence. As a result, analyses of crystallite alignment and distribution in starch granules, or of crystal structure dynamics during treatments, e.g. digestion or gelatinization, have been difficult. This limits the understanding of starch structure and greater utilization of starch.

Recent advances in birefringence imaging integration with other imaging techniques, such as quantitative phase microscopy (QPM) and digital holographic microscopy (DHM) (Coppola & Ferrara, 2020), may resolve some of these issues. DHM, an interferometric-based imaging method, enables non-destructive and label-free quantitative phase measurements of biological samples and microstructures (Ebrahimi, Moreno-Pescador, Persson, Jauffred, & Bendix, 2023; Kemper & Von Bally, 2008). In DHM, the relative orientation between two interfering beams, the beam which interacts with the sample and the reference beam, determines whether the system operates in on-axis or off-axis geometry. The on-axis mode features a simpler setup but often suffers from artifacts due to the overlap of the zero-order diffraction and twin images, necessitating time-consuming image acquisition and iterative data processing to remove artifacts. By contrast, the off-axis geometry introduces a tilt between the reference beam and the beam modulated by the sample, allowing for single-shot acquisition and thus faster measurements (Ebrahimi & Dashtdar, 2021). In polarization-based DHM, two holograms must be recorded using illuminations with two perpendicular polarization states of the reference wave. This approach combines the benefits of birefringence imaging with the rapid, quantitative capabilities of DHM, enabling more efficient and accurate analysis of microstructural dynamics in samples. A numerical method can then be employed to simultaneously reconstruct the amplitude, phase, and polarization information of the sample (Colomb et al., 2005).

Although the crystal type and crystallinity of starches have been extensively studied, traditional methods typically provide only the mean crystallinity of a starch sample. These methods are limited in visualizing the spatial distribution of crystalline domains within individual granules and in capturing the heterogeneity within one starch type. Such heterogeneity is critical for understanding key properties such as gelatinization and digestion. Birefringence imaging offers a means to visualize crystal distribution, but it is often limited in quantitative analysis. In this study, we applied a custom-built polarization-based DHM configuration to achieve quantitative birefringence and optical-axis orientation imaging of single starch granules, enabling in situ monitoring and quantification of starch digestion. The microscope takes advantage of a highly stable, common-path geometry using a Fresnel biprism (Ebrahimi, Dashtdar, Sánchez-Ortiga, Martínez-Corral, & Javidi, 2018; Yaghoubi, Ebrahimi, & Dashtdar, 2022). We further employed gradient light interference microscopy (GLIM) module to investigate the 3D structures of starch granules by scanning in different depths (Nguyen, Kandel, Rubessa, Wheeler, & Popescu, 2017). We showed that the polarization strength can be quantitatively understood using quantitative phase polarization microscopy method and proved that the crystal is not evenly distributed in the granules, thereby gaining a deeper understanding of starch structure. The enzymatic hydrolysis and digestion of gelatinized starch is also analyzed using the technique, enhancing insights into starch digestion processes.

2. Materials and methods

2.1. Materials

Six starch samples were used in this study, including three maize starches: waxy maize starch (WMS), purchased from Cerestar-AKV I/S (Denmark); normal maize starch (NMS), Commercial Clinton 106, from Archer Daniels Midland (ADM, Decatur, IL, USA); and high amylose maize starch (HMS), provided by the Maize Genetic Breeding Laboratory, Northwest A&F University, Yangling, China. Waxy, normal, and high amylose potato starches (WPS, NPS, HPS) were extracted in the laboratory as previously described (Guo et al., 2024; Tian et al., 2024). The amylose contents are WMS: 0.1%, NMS: 30.7%, HMS: 51.6%, WPS: 1.9%, NPS: 19.8% and HPS: 34.4%. Pancreatin (A7545) and amyloglucosidase (A7095) were purchased from Sigma-Aldrich (USA), while isoamylase (E-ISAMY, 200 U/mL) was obtained from Megazyme (Ireland). All other chemical reagents used in this study were sourced from Sigma-Aldrich (USA).

2.2. Starch structural characterization

2.2.1. Size exclusion chromatography (SEC)

The weight-based molecular weight distribution of native starch and the chain length distribution of isoamylase-debranched starch were analyzed using size exclusion chromatography coupled with a triple detector array (SEC-TDA, Viscotek, Malvern, UK) (Tian et al., 2024). The system was equipped with GRAM 1000 SEC columns (Polymer Standards Service GmbH, Mainz, Germany) and connected to a refractive index detector (PN3140, PostNova Analytics, Landsberg, Germany). For native starch analysis, samples (5 mg) were dissolved in 1 mL of DMSO/LiBr solution (0.5% w/w, Avantor, US) at 80 °C overnight. The solution was then centrifuged at 20,000*g* for 5 min, and the supernatant was injected into the SEC system. Elution was carried out using DMSO/LiBr at a flow rate of 0.5 mL/min with a column temperature of 65 °C. To prepare debranched starch samples, starch dispersions were heated in screw-capped tubes with DMSO/LiBr (5 mg/mL) at 80 °C for 3 h. Three volumes of absolute ethanol were added to the DMSO-dissolved starch system to precipitate the gelatinized starch, which was then collected by centrifugation at 4000*g* for 10 min and dried in a fume hood at ambient temperature. Debranching was performed by adding 2 μL of isoamylase

(0.4 U) to 1 mL of sodium acetate buffer (0.01 M, pH 4.0), incubating at 40 °C for 3 h, followed by freeze-drying. The debranched starch samples were then prepared at a concentration of 5 mg/mL for subsequent analysis. Samples dissolved in DMSO/LiBr were prepared before injecting onto the SEC system.

2.2.2. High-performance anion exchange chromatography-pulsed amperometric detection (HPAEC-PAD)

Isoamylase enzymatic debranching was performed as described in *SEC* and the debranched starch (40 μL, 5 mg/mL) was injected onto a CarboPac PA-200 column attached to an HPAEC-PAD (Dionex, Sunnyvale, CA, USA) system. Columns were pre-washed with 100 mM NaOH at 0.4 mL/min for 20 min. The elution process made use of three solutions: MilliQ water (eluent A), 1 M NaOH (eluent B), and 1 M NaOH enriched with 25 mM NaAc (eluent C). The elution gradient functioned at a rate of 0.4 mL/min and proceeded in the following manner: an initial phase of 0–5 min (with 15% of eluent A and 85% of eluent C), followed by 5–130 min (where eluent B increased linearly to 40% and eluent C dropped linearly to 45%), 130–135 min (with 80% eluent A and 20% eluent C), and lastly from 135 to 145 min (reverting to the original eluent mixture). Peak integration and detector response were performed as described (Tian et al., 2024).

2.2.3. Wide angle X-ray scattering (WAXS)

After conditioning the samples in a humidity chamber at 90% relative humidity with saturated KCl for 72 h, the samples were analyzed using a Nano-inXider instrument (Xenocs SAS, Grenoble, France) under the conditions of a 40 mA current, 40 kV voltage, and 0.1542 nm wavelength Cu Kα radiation. The radial average intensity, I, was measured as a function of the scattering angle 2θ within the range of 5–40°. The relative crystallinity was calculated using PeakFit software (version 4.12, Systat Software, Inc., San Jose, CA, USA), which estimated the amorphous background scattering. The relative crystallinity (%) was determined by the formula: Relative crystallinity (%) = (Peak areas/Total area) (Tian et al., 2024).

2.2.4. Small-angle X-ray scattering (SAXS)

The nano-lamellar structure of starch was analyzed using a Nano-inXider instrument (Xenocs SAS, Grenoble, France). Starch powder was dissolved in excess MilliQ water and incubated at 4 °C overnight. The resulting suspension was centrifuged at 5000*g* for 5 min, after which the supernatant was removed. The remaining suspension (0.7 mL) was then transferred to 1-mm-thick sample cells for further measurement. The data fitting, including the determination of the thickness of crystalline (dc) and amorphous (da) lamellae, was performed using a previously described method (Tian et al., 2024).

2.2.5. Fourier transform infrared - attenuated total reflectance (FTIR–ATR) spectroscopy

FTIR–ATR spectroscopy was conducted using a Bomem MB100 FTIR spectrometer equipped with a Golden Gate attenuated total reflectance (ATR) accessory. The starch samples were first equilibrated to the ambient laboratory humidity. Spectra were collected at a resolution of 4 cm^{-1}, with co-added scans for each sample. Background spectra were obtained by cleaning the ATR crystal with a mixture of ethanol and water, followed by recording 128 co-added scans. A Lorentzian line shape with a half-width of 19 cm^{-1} and a resolution enhancement factor of 1.9 was applied. After performing baseline correction and deconvolution analysis using OMNIC software, the IR absorbance values at 1022 and 1045 cm^{-1} were extracted from the spectra (Tian et al., 2024).

2.3. Multimodal bright-field (BF), polarization, differential interference contrast (DIC) and quantitative-phase digital holographic microscopy (DHM)

The polarization light microscopic visualization of starch granules was performed using an inverted light microscope (Nikon, Eclipse Ti2) under bright-field, dark-field polarized and differential interference contrast (DIC) modes at cross-polarization state. GLIM module (Phi Optics Inc), mounted on the microscope output was used for QPM acquisitions and 3D phase imaging by z-scanning. The GLIM module integrates DIC with low-coherence, common-path digital holography, effectively suppressing multiple scattering and speckle noise artifacts and enabling time-lapse imaging of thick specimens. Its strong optical-sectioning capability also supports tomographic imaging. By precisely adjusting the phase difference between the two interfering beams via a spatial light modulator, multiple intensity images are acquired, which are then used to generate phase-gradient maps and, eventually, a quantitative phase map through integration along the phase shift direction. A 20× microscope objective lens (Plan Apo, $NA = 0.75$) was used for multimodal imaging and the images were captured by a sCMOS camera (Hamamatsu, ORCA Flash4.0, 2048 × 2048 pixel array and 6.5 μm pixel-pitch).

Additionally, a common-path digital holographic microscopy setup was implemented based on the Fresnel biprism nearly off-axis geometry and 4f optical filtering system to quantify the birefringence retardance and optical axis orientation of starch granules. A schematic configuration of the setup is shown in Fig. S5.

2.4. In situ analysis of starch enzymatic hydrolysis and digestion by QPM

A GLIM protocol was employed for dynamic investigation of phase changes in gelatinized starch granules through enzymatic digestion. This QPM technique combines DIC microscopy with low-coherence interferometry and holography and achieves quantitative polarization-sensitive tomographic images of both thin and thick samples by optical sectioning. The possibility of real-time imaging of the technique makes it a powerful candidate for screening dynamic phenomena. A 40× microscope objective lens (Plan Apo, $NA = 0.95$) was used for this measurement. Depending on the starch digestion rate, time-lapse images were captured at acquisition rates of 1 Hz–10 Hz and for acquisition times of a few hundred seconds to a few thousand seconds.

2.5. Statistical analysis

All experiments were conducted in triplicate, and the data are presented as mean ± standard error. The normality of the data was assessed using the Shapiro-Wilk test, which confirmed that the data followed a normal distribution. Pearson's correlation analysis was applied to assess linear relationships between variables, with the understanding that nonlinear relationships may not be captured by this method. Statistical significance was determined using Duncan's post hoc test at a 95% confidence level ($p < 0.05$). All analyses were performed using SPSS 20.0 (SPSS Inc., Chicago, IL).

3. Results and discussion

3.1. Multi-scale structures of maize and potato starches with different amylose content

To link features of starch granules, such as molecular structure (Fig. S1, Fig. S2, Table S1, and Table S2), lamellar structure (Table S3), crystalline structure (Fig. S3 and Table S3), and granular surface structure (Fig. S4 and Table S3) with data from our custom-built microscope, we first characterized the starch granules according to the following:

3.1.1. Chain length distributions (CLDs) of starches as analyzed by SEC and HPAEC-PAD

Size-exclusion chromatography (SEC) analysis of starch samples are shown in Fig. S1A and Table S1 (Hernández et al., 2008; Zhong, Liu, et al., 2020b). Here, we found that WMS contained a higher proportion

of molecules with large hydrodynamic radii, reflecting the dominance of amylopectin fractions. NMS showed a broader size distribution, indicating the presence of both amylopectin and amylose. HMS displayed a bimodal size distribution, corresponding to the higher amylose content. Similar trends were observed in potato starches, where WPS resembled WMS, while NPS and HPS showed broader and bimodal distributions, respectively.

Debranching (with subsequent SEC analyses) (Fig. S1B and Table S1) revealed that WMS contained mainly short amylopectin chains, with no detectable amylose. NMS displayed a wider range of chain lengths, with both short amylopectin chains and long amylose chains. HMS showed a significant shift towards longer chain lengths, with amylopectin chains being more evenly distributed, and a clear presence of long amylose chains, contributing to the bimodal distribution. In the potato starches, WPS exhibited a pattern similar to WMS, dominated by short amylopectin chains. NPS showed a wider distribution, and HPS presented a profile dominated by long chains, indicative of a high amylose content disrupting the regular amylopectin structure.

HPAEC analysis (Fig. S2 and Table S2) (Lim, Zhang, Ferruzzi, & Hamaker, 2019; Zhong, Bertoft, Li, Blennow, & Liu, 2020) revealed that WMS was dominant in short chains (fa, DP 6–12), with few intermediate and long chains. NMS exhibited a more balanced distribution of chain lengths, with a noticeable presence of both short (fa) and longer chains (fb1, fb2). HMS was characterized by a high proportion of fb1 chains and less fb3 chains. In potato starches, WPS showed patterns similar to WMS, dominated by short chains. NPS contained both short and long chains, and HPS exhibited the highest proportion of fb1 chains and lowest fb3 chains.

3.1.2. Crystalline structure and lamellar structure

To understand how amylose and amylopectin contribute to granular architecture, Small-angle X-ray scattering (SAXS) was employed to analyze lamellar structures (Table S3). The effects of amylose on lamellar organization were found to be crop-dependent. For maize starches, WMS exhibited a total lamellar thickness (dac) of 9.2 nm, with crystalline (dc) and amorphous (da) lamellae of 7.2 and 2.1 nm, respectively. With increasing amylose content, NMS showed only minor changes (dac = 9.3 nm, dc = 7.6 nm, da = 1.7 nm), whereas in HMS a reduction in dac (9.1 nm) and dc (7.1 nm) accompanied by an increase in da (1.9 nm) was observed, indicating disruption of lamellar packing in an intrinsically less ordered structure. In contrast, potato starches showed a different trend. WPS displayed dac, dc, and da values of 8.8, 6.7, and 2.1 nm, respectively. In NPS, dac and dc decreased to 8.4 and 6.1 nm, while da slightly increased to 2.2 nm. Notably, HPS exhibited increased dac (9.1 nm) and dc (7.0 nm), suggesting an expansion or reinforcement of the lamellar structure.

Wide-angle X-ray scattering (WAXS) (Fig. S3 and Table S3) provides data on crystalline polymorphs and relative crystallinity, revealed that WMS and NMS predominantly exhibited an A-type crystalline structure (Yang, Gu, & Hemar, 2013), representing a compact double-helix typical of cereals. By contrast, HMS shifted to a more hydrated B-and V-type crystalline structure, attributed to long amylopectin side chains associated with amylose (Tian et al., 2024). Potato starches (WPS, NPS, HPS) consistently exhibited a B-type crystalline structure (Dankar, Haddarah, Omar, Pujolà, & Sepulcre, 2018), typical of tuber starches. As amylose content increased, the crystallinity decreased across both maize and potato starches. In WMS, crystallinity was 14.4%, decreasing to 11.6% in NMS, and further dropping to 8.5% in HMS. For potato starches, WPS exhibited the highest crystallinity at 17.0%, which decreases to 16.1% in NPS and 14.7% in HPS.

3.1.3. Surface order degree

We finally used FTIR spectroscopy to gain insights into the relative ordering of the crystalline and amorphous regions of starch granules, specifically the 1045/1022 cm^{-1} ratio (Table S3) (Warren, Gidley, & Flanagan, 2016). A higher ratio indicates a greater degree of crystalline order, while a lower ratio suggests a more amorphous structure. In WMS, the 1045/1022 ratio was 0.73. In NMS, the ratio decreased to 0.69, and in HMS, it further decreased to 0.67. For potato starches, WPS showed a ratio of 0.87, which decreased to 0.83 in NPS, and then slightly increased to 0.87 in HPS.

3.2. A custom-built DHM configuration provides insights into the crystal distribution within starch granules

To quantify birefringence of starch granules, we developed a polarization-based DHM method (Fig. S5). The system employs a diode laser with a wavelength of 650 nm and coherence length of a few millimeters as the light source. A 1-in. right-handed circular polarizer (Thorlabs, central wavelength 633 nm) was used to generate the required input circular polarization sate. A Fresnel biprism, made from BK7 glass (refractive index of 1.51) with the dimension of 60 × 40 mm and the refringence angle of 0.07 rad and positioned 60 mm from the microscope objective rear aperture in the microscope's optical path, splits the wavefront into two overlapping beams through refraction phenomena resulting in an off-axis imaging geometry (Ebrahimi et al., 2018; Ebrahimi, Dashtdar, Fonda, & Cabrera, 2025; Goodwin, Lim, Mahajan, & Nolte, 2025). A rotating film polarizer (Thorlabs, 0.5-in. diameter, wavelength range 400–700) was inserted in the reference wave path to produce the orthogonal polarization states. The holograms were recorded by a FLIR CMOS sensor (1920 × 1200 pixels, pixel size 5.86 μm). This design is highly compact and readily adaptable for integration with lab-on-a-chip platforms (Ballard, Zhang, & Ozcan, 2017; Merola et al., 2015). By using a single illumination beam, the setup enables off-axis polarization digital holographic imaging without requiring additional optical components such as mirrors and beam-splitters (Tsai, Vyas, & Luo, 2024). Its common-path geometry provides enhanced robustness against vibrations, environmental disturbances, and optical misalignment (Anand, Chhaniwal, & Javidi, 2018). The polarization sensitivity of the system facilitates simultaneous holographic imaging of orthogonal polarization components in birefringent specimens and supports quantitative extraction of two-dimensional birefringence metrics, including phase retardation and optic-axis orientation (Coppola & Ferrara, 2020).

A hologram image of a starch granule is shown in Fig. 1(a). The interference pattern includes three-dimensional structural information of the starch granule coupled with refractive index distribution i.e., optical path length information. The concentric rings visible in the hologram suggest layered structures within the granule, indicating variations in thickness or refractive index that cause phase shifts in the transmitted light. The method provides a direct way to visualize the internal morphology of the granule without any labeling or staining via two separate image acquisitions performed at orthogonal polarization states. The holograms were reconstructed by Fourier transform analysis method. Via 2D fast Fourier transform, the spatial information of hologram can be transformed into frequency space (Fig. 1(b)). The highlighted red circle indicates the first diffraction order corresponding to the structural feature in the granule, such as lamellae or other periodic arrangements. This component's prominence suggests a dominant structural motif, which can be linked to the organization of amylopectin and amylose chains within the granule. After windowing the first diffraction order and shifting the filtered spectrum to the center, an inverse Fourier transform results in the reconstruction of the amplitude distribution and phase delay. A second hologram was then captured at 90-degree rotation of reference beam polarization (See Fig. S5) with subsequent reconstruction. By either subtracting or averaging the two obtained phase distributions we obtained both the birefringence phase retardation (Fig. 1(c)) and optical axis orientation (Fig. 1(d)) (see supplementary file for the mathematical descriptions). Birefringence occurs when light passes through an anisotropic material, like a starch granule with aligned crystalline regions, causing different phase delays for different polarization states. The color-coded map shows the retardance

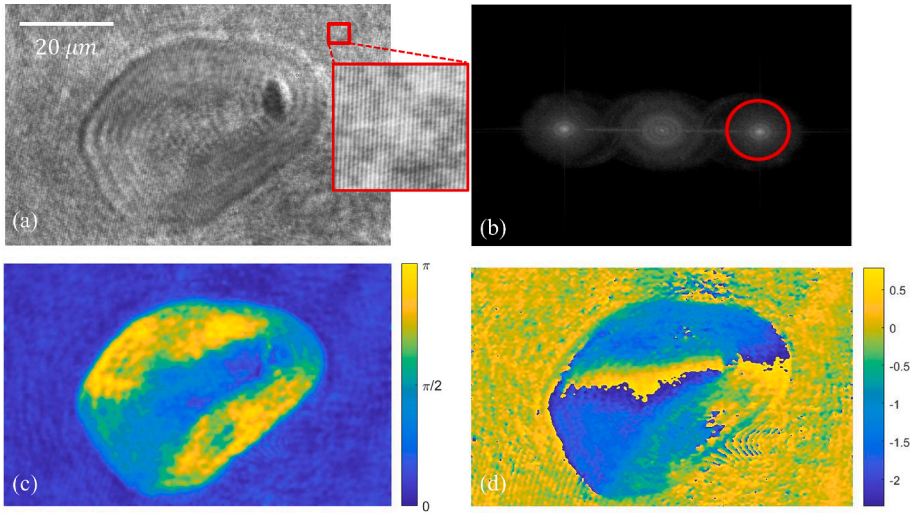

Fig. 1. Holographic imaging pipeline. (a) A raw hologram of a normal potato starch granule. (b) Fourier spectrum of (a). (c) Birefringence and (d) optical axis orientation maps, obtained by Fourier transform analysis and filtering the first diffraction order (the red circle in (b)) in Fourier domain. The color bar shows the phase delay in radian. (For interpretation of the references to color in this figure legend, the reader is referred to the web version of this article.)

angle in radians, with distinct regions of high and low birefringence (Fig. 1(c)). These variations reflect differences in crystalline order within the granule, with higher values (yellow regions) indicating more organized structures and lower values (blue regions) representing areas with higher amorphous content. The optical axis orientation map visualizes the vibration directions of the crystals relative to the optical axis, indicating the alignment of molecular structures. The color gradients represent different orientations of the optical axis in radian, which should correspond to the directions in which amylopectin chains are aligned. This information is crucial for understanding how the internal crystalline and amorphous regions are spatially organized and how they might interact with light under polarized conditions. Fig. 2 shows the birefringence maps for three different potato starch types, waxy, normal and high amylose. Here, the high-amylose starch shows a lower birefringence retardance compared with those of waxy and normal types.

To further investigate how starch structural parameters influence birefringence intensity, we calculated the mean birefringence intensity of 17 individual granules for each starch type (Fig. S6), and analyzed its correlation with starch structural parameters (Fig. 3). The mean value was calculated by averaging the local birefringence within the regions occupied by granules. When the correlation analysis was performed separately for the two crops, birefringence intensity exhibited a positive correlation with RC_{deAP1} and $RC_{na\text{-}AP}$, and a negative correlation with ACL_{deAP1}, ACL_{deAP2}, and $RC_{na\text{-}Am}$. These findings highlight a critical role of molecular structural parameters in determining birefringence intensity. Specifically, they underscore the importance of amylopectin, particularly the content and lengths of amylopectin short chains, in forming a more ordered birefringent structure, while amylose disrupts this order (Zhong, Liu, et al., 2020a). When correlation analysis was performed using combined data from both crops, birefringence intensity showed a positive correlation with crystallinity and Rh-AM average, and a negative correlation with RCna-Am. These relationships suggest that birefringence intensity is primarily influenced by aggregated structural features, including overall crystallinity and molecular size. Differences observed between crop-specific and combined analyses mainly arise from substantial variations in molecular and supramolecular organization between maize and potato starches, which affect the direction and strength of the correlations. This reflects the multi-level influence of starch structure on functionality, with both molecular features (e.g., amylopectin chain length) and aggregated structures (e.g., crystallinity, crystalline lamellar thickness) contributing to functional outcomes in a crop-specific manner. Overall, the results indicate that birefringence intensity is jointly controlled by molecular and aggregated structures, especially the content of amylopectin ($RC_{na\text{-}Ap}$), with the effects varying based on crop origin and structural scale. However, some starch structural features, such as surface roughness, which are difficult to quantify, might also play an important role in the observed birefringence differences.

3.3. *Increasing amylose content leads to a more heterogeneous internal crystalline distribution of starch granules*

To validate our findings obtained from the custom-built birefringence technique, we studied the morphology of starch granules using a multi-modal commercial Nikon microscope that integrates Bright Field (BF), Polarized Microscopy (PM), Differential Interference Contrast (DIC), and Quantitative Phase Microscopy (QPM) techniques (Fig. 4). Here, we aimed to understand how amylose content and botanical

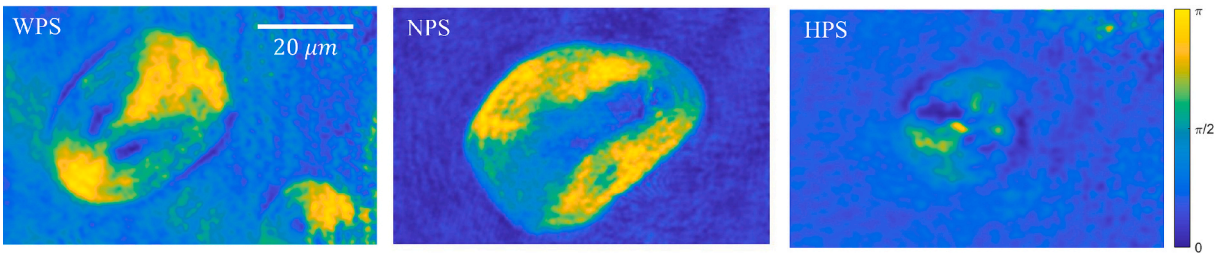

Fig. 2. Birefringence phase delay images of potato starches with different amylose content, including waxy starch (left), normal starch (mid), and high amylose starch (right). The color bar shows the phase delay in radian.
WPS: waxy potato starch; NPS: normal potato starch; HPS: high-amylose potato starch. Note: the image of NPS is the same as in Fig.1c as conditions are identical.

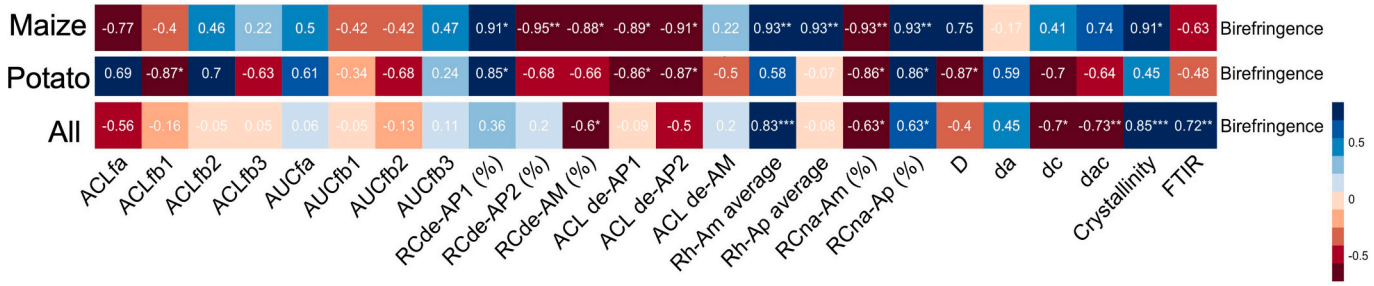

Fig. 3. The correlation between birefringence from the microscopy and starch structural parameters. $RC_{de\text{-}X}$: relative amount of fraction X of debranched sample; $RC_{na\text{-}X}$: relative amount of fraction X of native sample; $ACL_{de\text{-}X}$: the average chain length (DP) of the fraction X of debranched sample; $Rh_{na\text{-}X}$: hydrodynamic radius of fraction X of native sample. RC_X: relative mount of fraction X of debranched samples; ACL_X: verge chin lengths (DP) of fraction X of debranched samples; fa: amylopectin chains with DP 6–12; fb1: amylopectin chains with DP 13–24; fb2: amylopectin chains with DP 25–36; fb3: amylopectin chains with DP >36. D, Bragg lamellar repeat distance; d_{ac}, d_a and d_c, the thicknesses of total, amorphous, and crystalline lamellae, respectively; FTIR: the ratio of 1045/1022 cm^{-1}. *, **, and *** indicate significant correlations at $p < 0.05$, 0.01, and 0.001 levels, respectively.

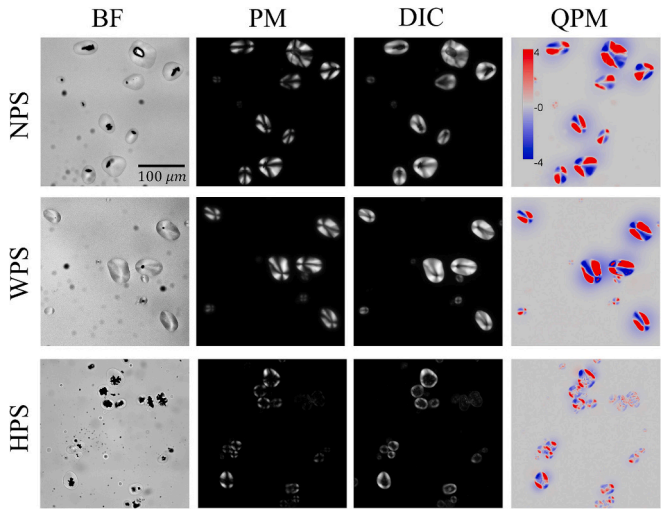

Fig. 4. Microscopic imaging of potato starch granules using BF, PM, DIC, and QPM techniques. BF: Bright Field, PM: Polarization Microscopy, DIC: Differential Interference Contrast, and QPM: Quantitative Phase Microscopy. In QPM, the color bar represents the gradient of optical phase, with red indicating regions of higher optical path length, and blue indicating lower optical path length.
WPS: waxy potato starch; NPS: normal potato starch; HPS: high-amylose potato starch. (For interpretation of the references to color in this figure legend, the reader is referred to the web version of this article.)

source affect the crystal distribution of starch. For waxy and normal potato starch granules, BF imaging showed large, oval granules with a relatively uniform size distribution, indicating a consistent granule morphology. PM images revealed distinct Maltese cross patterns, indicative of strong birefringence and a highly ordered internal crystalline structure, characteristic of amylopectin-rich regions. DIC imaging provided a more nuanced view by highlighting subtle variations in surface texture and internal structure that are not visible in BF or PM images. The DIC images displayed distinct shading and contrast variations across the granule surfaces, which correspond to differences in refractive index and surface topology. These shading patterns indicate that the granules have an anisotropic distribution of surface irregularities, with certain regions showing more pronounced contrast changes than others. This suggests that the granules exhibit directional variations in microstructural features, such as zones of differing crystallinity or packing density, potentially aligned along specific orientations related to the granule's growth or the organization of amylopectin chains. QPM further complemented these findings by providing a quantitative phase map of the granules, illustrating how light is phase-shifted as it passes through different parts of the granule. The QPM images revealed distinct color gradients corresponding to variations in optical path length differences, indicating regions of differing refractive index. Notably, QPM highlighted a directional distribution of crystallinity within the granules, with higher phase shifts concentrated at two opposite ends of the granules and lower phase shifts on the other two ends. This pattern indicates that crystalline regions are positioned on both sides of the granules, with non-crystalline material extending radially in between, possibly aligning with the granule's growth direction or the orientation of amylopectin branches. For high-amylose potato starch granules, BF imaging revealed granules with highly irregular shapes, differing significantly from the more uniform shapes of waxy and normal starch granules. PM imaging showed significantly reduced birefringence, with an absence of the clear Maltese cross patterns observed in the other starch types, indicating a lack of internal crystalline order and a higher degree of amorphous structure. DIC imaging provided detailed contrast of the granules' rough surfaces, highlighting significant variations in surface topology and thickness, reflecting a more disordered internal structure and uneven packing. QPM further revealed highly heterogeneous phase shift distributions, characterized by abrupt color changes, suggesting significant internal differences in density and refractive index, likely due to the high amylose content disrupting the crystalline regions and creating a more amorphous internal composition.

Waxy maize starch granules displayed uniform polyhedral shapes, distinct Maltese cross patterns under PM, and minimal surface roughness and structural disruptions, as seen in BF, DIC, and QPM imaging (Fig. 5). The crystalline regions were concentrated at the granule ends, showing ordered internal composition. In contrast, normal maize starch granules exhibited smaller, irregular shapes, reduced birefringence, and more pronounced surface roughness, indicating increased morphological variability. QPM showed uneven phase shifts, reflecting differences in internal refractive indices and amylose's less ordered distribution. High-amylose maize starch granules had highly irregular shapes, minimal birefringence, and significant surface roughness, indicating a largely amorphous structure. QPM revealed highly heterogeneous phase shifts, with variations in density and refractive index, pointing to both dense, amylose-rich amorphous areas and occasional crystalline pockets. The results underscore the significant impact of amylose content on starch granule structure, from waxy starch with a highly ordered crystalline structure to high-amylose starch with a more disrupted, heterogeneous internal composition.

While the impact of increasing amylose content on starch structure shows similar trends for the two botanical sources studied (maize and potato), some distinct differences arise due to their unique granule architectures. Potato starch granules are generally larger with more complex surface features, which are highlighted by DIC and QPM imaging. DIC reveals significant surface roughness and pronounced height variations in potato starch granules, suggesting a more heterogeneous

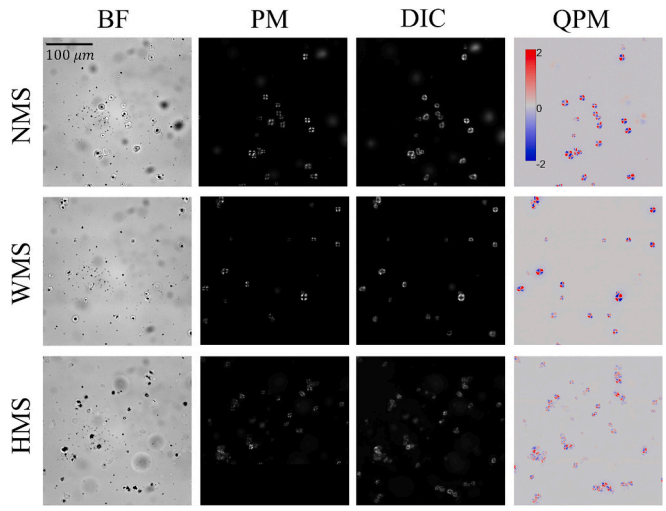

Fig. 5. Microscopic imaging of maize starch granules using BF, PM, DIC, and QPM techniques. BF: Bright Field, PM: Polarization Microscopy, DIC: Differential Interference Contrast, and QPM: Quantitative Phase Microscopy. In QPM, the color bar represents the gradient of optical phase distributions.
WMS: waxy maize starch; NMS: normal maize starch; HMS: high-amylose maize starch.

surface structure and internal packing. This complexity in surface texture could result from the unique way, amylopectin and amylose are organized within potato starch granules, creating varied refractive index regions. In contrast, maize starch granules are smaller and more compact, with DIC imaging showing smoother surfaces and more uniform thickness. However, in high-amylose maize starch, there is more evident granule aggregation, suggesting stronger inter-granular interactions, potentially due to different surface properties influenced by higher amylose content. This clustering tendency could reflect differences in how amylose and amylopectin interact at the granule surfaces in maize compared to potato. QPM further distinguishes the two starch types by revealing differences in internal composition. Potato starch shows varied phase shift patterns within granules, indicating heterogeneous internal structures with regions of different densities and refractive indices. This suggests more localized variations in crystalline and amorphous regions within potato granules. By contrast, maize starch granules, particularly at high amylose levels, exhibit more uniform phase shifts within individual granules but greater variability between granules, indicating a more consistent internal composition within each granule but a broader range of granule types. Overall, the botanical origin influences starch granule properties, with potato starch having more heterogeneous surface and internal structures while maize starch showing more uniform but clustered granule behavior.

3.4. 3D visualization of starch granules via QPM microscopy reveals crystal distribution consistent with the patterns observed in 2D visualization

To understand the internal optical heterogeneity and organization of the granules, the 3D visualization of potato starch granules was shown in Fig. 6. In waxy and normal starch granules, the crystalline regions are prominently distributed on both sides and remain consistent along the z-axis, indicating a well-ordered internal network with varying birefringence. By contrast, high-amylose starch granules appear more uniformly colored with minimal variation, suggesting a predominantly amorphous structure due to amylose disrupting the crystalline order. This 3D view provides deeper insights into how amylose content affects the structural and optical properties of starch, enhancing our understanding of granule organization in three dimensions.

3.5. The crystalline regions in starch granules are aligned in specific directional patterns

More detailed insights into starch structure, particularly the alignment of crystalline regions was obtained by using DIC and QPM. DIC shows that starch granules have crystalline regions distinctly distributed on both sides of granule, maintaining consistency along the z-axis, while non-crystalline regions extend radially between these two regions. This suggests a highly ordered alignment along one axis, consistent with the layered arrangement of crystalline lamellae, while the other axes appear more disordered due to the presence of amorphous regions. These amorphous areas, often disrupted by amylose or longer amylopectin chains, are less ordered and distributed randomly. The higher crystalline order along a specific axis indicates that amylopectin molecules are more tightly packed and aligned in that direction, while amylose disrupts this alignment, contributing to increased structural disorder in the perpendicular directions.

There are two main models describing how AP chains are organized in the branched polymer: the “cluster model” (Nikuni, 1978) and the “building block backbone model” (Bertoft, 2017). The key difference between them is that in the cluster model, long AP chains penetrate both crystalline and amorphous lamellae, while in the building block backbone model, the chains are primarily oriented within the amorphous lamellae, with some extending into the crystalline regions (Zhong et al., 2022). In the cluster model, short AP chains are densely packed together by branch points in the amorphous lamella, and longer parallel AP chains connect these clusters in a radial arrangement within the starch granule (Zhong et al., 2022). However, these models primarily focus on the alignment of amylopectin, while the alignment of crystallites remains unclear. It is generally assumed that the crystals are evenly distributed in all directions within the granules (Pérez & Bertoft, 2010; Wang & Copeland, 2015), although this assumption has been debated and lacks experimental evidence. By combining DIC and QPM microscopy, we provide the first experimental data showing that the crystalline structure follows a clear directional alignment, with possible disordered crystals and amorphous regions in other directions. This

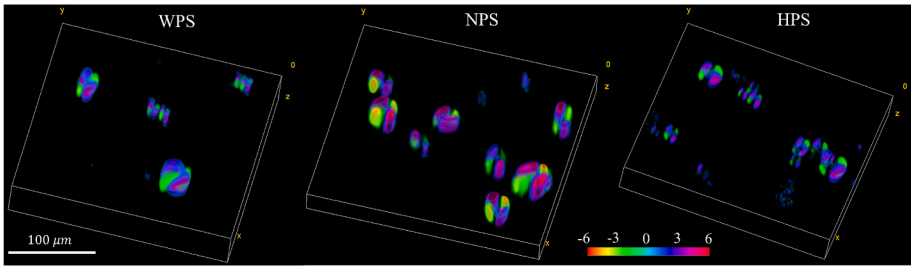

Fig. 6. Three-dimensional imaging of phase gradience in potato starch granules. The color bar represents optical phase shifts (in radians).
WPS: waxy potato starch; NPS: normal potato starch; HPS: high-amylose potato starch.

helps explain why starch granules have relatively low crystallinity, typically below 20%, as seen in maize and potato starches used here. Although the microscope analysis is unable to observe molecular organization directly, our data may contribute to refining the two well-recognized starch structure models, i.e., the cluster or backbone model. Furthermore, it helps clarify that amylose disrupts the granular structure by weakening the clear directional alignment of the crystalline structure.

3.6. The heterogeneity of crystalline structure affects thermal behavior of granules

New information on starch granular heterogeneity was provided by the multimodal characterization, and helps understanding the starch functionality, e.g., thermal and enzymatic hydrolysis properties. It is well known that starch granules exhibit a wide range of sizes, shapes and polarization patterns, leading to questions about whether granular structures influence starch functionality, including gelatinization and digestion. While some studies have provided evidence in this area (Cai et al., 2014; Corgneau et al., 2019; Pérez, Baldwin, & Gallant, 2009; Wei et al., 2010), our data reveal a different aspect of starch granule heterogeneity. As shown in the QPM images in Figs. 4 and 5, the crystalline ordering varies between granules of the same starch type, regardless of their size and shape. This helps in understanding starch functionality, e.g., thermal properties and enzymatic reactions. The broad DSC peak traditionally interpreted as a gradual melting process within individual starch granules, from onset to final temperature (Biliaderis, Page, Maurice, & Juliano, 1986; Genkina, Kozlov, Martirosyan, & Kiseleva, 2014; Ratnayake & Jackson, 2008), may instead result from variations in crystalline structure between granules. From our data, we propose that rather than each granule melting progressively, some granules may melt rapidly at different points within this temperature range. This broad peak reflects the heterogeneity in crystalline ordering among granules, with some melting closer to the onset temperature and others near the final temperature, rather than a continuous process within a single granule. The substantial impact of crystal alignment heterogeneity on starch enzymatic hydrolysis and digestion is further discussed in the following two sections.

3.7. Enzymatic hydrolysis leads to gradual breakdown of amorphous and crystalline phases

The enzymatic hydrolysis of normal maize starch granules was further examined using QPM with a high dosage of *amyloglucosidase* (AMG), which allows monitoring granular disruption within a short time. AMG is widely used as a model digestive enzyme in in vitro experiments and is known to degrade native starch and produce porous structures (Genyi, Zihua, & Hamaker, 2006; Han et al., 2021). Time-lapse visualization captures dynamic changes in granule structure during hydrolysis, revealing real-time alterations in internal organization and optical properties (Fig. 7). At the initial stage (0 s) (Fig. 7a), the granules show distinct phase shifts with red and blue gradients, indicating a heterogeneous internal structure with varying refractive indices and densities. These patterns suggest a mix of crystalline and amorphous regions within the granules. As hydrolysis progresses, the phase shift variations diminish, reflecting the gradual breakdown of both crystalline and amorphous phases. The QPM data indicates that the enzymatic action begins at the granule surface, gradually penetrating inward, as evidenced by the initial changes occurring predominantly at the periphery of the granules. This suggests that *amyloglucosidase* attacks the starch granules from the outside inwards. Additionally, the images do not show a preferential attack on either crystalline or amorphous regions; instead, they suggest that the enzyme acts simultaneously on both, leading to a uniform reduction in structural order throughout the granules. In Fig. 7b, the granules exhibit reduced color intensity, indicating a more homogeneous internal composition as the enzyme disrupts both the crystalline and amorphous regions. After 150 s, the minimal remaining color variations signify nearly complete granule disintegration, with a uniform low-density distribution of hydrolyzed starch components (see the Fig. 7c, showing the temporal phase decay for the granule specified by black dashed line in Fig. 7a).

The starch hydrolysis kinetics by *amyloglucosidase* has been investigated previously, which quantified the enzyme attack sites and the density of binding sites on starch granules (Tian et al., 2023). However, it did not address how these attack sites are distributed across the granular surfaces, particularly within crystalline or amorphous regions. This QPM visualization uniquely allows for quantitative and dynamic monitoring of structural changes, providing a deeper understanding of how enzymatic activity targets different regions within starch granules and the efficiency of hydrolysis across varying granule types. This reveals that *amyloglucosidase* does not selectively target crystalline or amorphous zones but instead uniformly attacks the entire granule structure from the surface inward (Evers, 1971; Genyi et al., 2006; Shrestha et al., 2012). This provides a comprehensive view of the enzymatic breakdown process in real-time, highlighting the interactions between amyloglucosidase and the starch granule's internal structure, leading to a deeper understanding of the hydrolysis dynamics. However, the dosage of AMG and differences in starch granules from various botanical sources may influence the degradation pattern, which warrants further investigation in future studies.

3.8. QPM allows monitoring the digestion of starch granules

An analysis of normal maize starch granule digestion was also conducted by QPM in Fig. 8 by using a mixture of amyloglucosidase and alpha-amylase in a low dosage that used in vitro digestion protocol

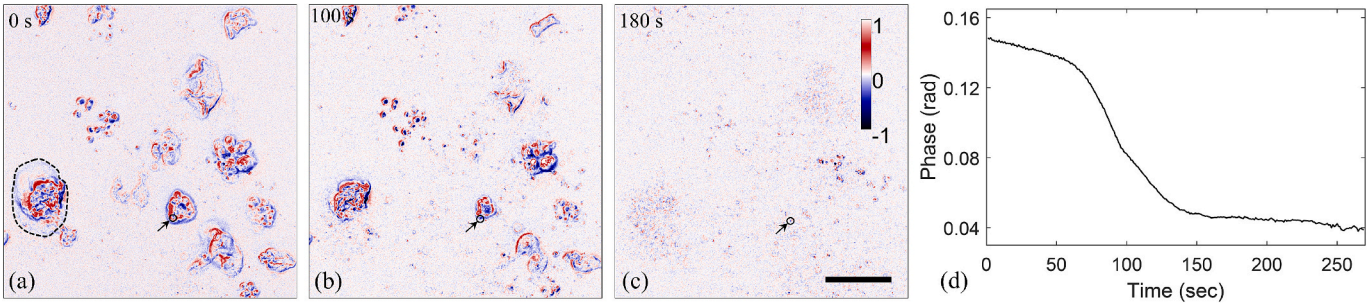

Fig. 7. (a–c) Time-lapse QPM images showing the degradation of normal maize starch granules over time during high-dosage amyloglucosidase hydrolysis and (d) the corresponding phase decay profile for the granule specified by black dashed line in the first panel from the left. A total of 270 images were collected during the experiment at an acquisition rate of 1 FPS over 270 s. The color bar represents the optical phase shift in radian, with red indicating higher optical phase and blue indicating lower optical phase. The scale bar represents 50 μm. (For interpretation of the references to color in this figure legend, the reader is referred to the web version of this article.)

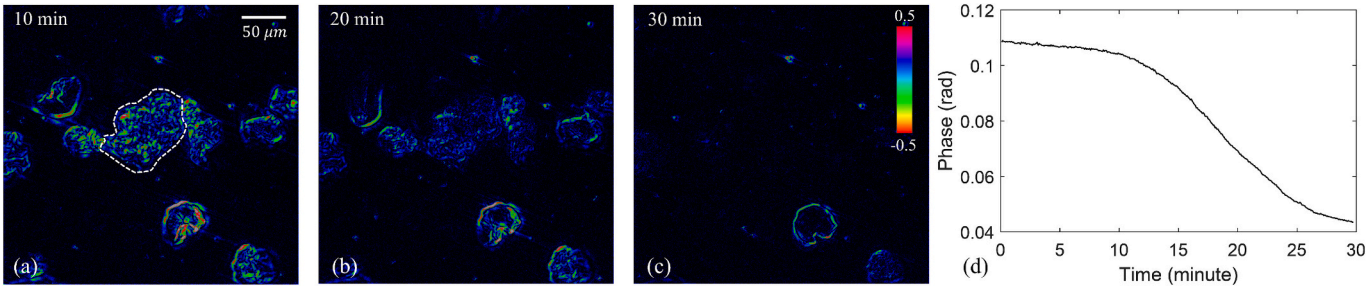

Fig. 8. (a–c) Time-lapse QPM images showing the in vitro digestion of normal maize starch granules decays over time and (d) the corresponding phase decay profile for the granule specified by white dashed line in the first panel from the left. A total of 360 images were collected during the experiment at an acquisition rate of 0.2 FPS over 30 min. The color bar represents the optical phase shift in radian, with red indicating higher optical phase and blue indicating lower optical phase. (For interpretation of the references to color in this figure legend, the reader is referred to the web version of this article.)

(Zhong, Liu, et al., 2020b) over time. This sequential visualization captures the dynamic changes in granule structure during the combined enzymatic hydrolysis, revealing notable differences in the digestion patterns compared to amyloglucosidase alone. At 10 min, the granules exhibit distinct phase shift patterns, with prominent color gradients indicating areas of high optical density and internal organization (Fig. 8a). These gradients suggest that the initial enzymatic action targets specific regions within the granules, possibly beginning at both the surface and partially inside, reflecting the combined effect of alpha-amylase and amyloglucosidase. After 20 min, there was a marked reduction in phase shift variation and color intensity (Fig. 8c), indicating an accelerated breakdown of both crystalline and amorphous regions compared to amyloglucosidase alone (see the Fig. 8d, showing the temporal phase decay for the granule specified by white dashed line in left panel). The faster reduction in optical heterogeneity suggests that alpha-amylase rapidly cleaves the internal starch structure, complementing the outer-to-inner hydrolytic action of amyloglucosidase. The "inside-out" digestion pattern of maize starch is consistent with previous studies. The combined action of alpha-amylase and amyloglucosidase leads to a quicker overall degradation process. At 30 min, the granules showed minimal remaining color variations, signifying near-complete disintegration (Fig. 8c). The mixed enzyme treatment suggests a synergistic effect where alpha-amylase rapidly degraded internal structures while amyloglucosidase continued its outer-to-inner action. This QPM visualization distinctly shows that the combination of amyloglucosidase and alpha-amylase led to a more effective and quicker enzymatic hydrolysis of starch granules, compared to amyloglucosidase alone. The data emphasize how the combined enzymes enhanced the breakdown of both the crystalline and amorphous regions, providing a more comprehensive understanding of the digestion dynamics under mixed enzymatic conditions.

4. Conclusion

Using a custom-built polarization-based DHM and a multimodal polarization microscope we map the heterogeneous structure of individual starch granules. Crystalline regions are consistently distributed in 3D space in a symmetrical way, with non-crystalline material extending radially in between. This directional crystalline alignment of high amylose starches is disrupted by amylose, which may interfere with the ordered structure. In situ analysis of enzymatic hydrolysis and starch digestion demonstrated that this crystalline heterogeneity leads to asynchronous breakdown of granules of the same starch type. However, additional biochemical validation, such as enzymatic digestion of pure amylose and amylopectin, will be needed in the future. These findings provide a more comprehensive understanding of the intricate organization and functional properties of starch granules.

CRediT authorship contribution statement

Samira Ebrahimi: Writing – review & editing, Writing – original draft, Software, Methodology, Investigation, Data curation, Conceptualization. **Yu Tian:** Writing – review & editing, Writing – original draft, Methodology, Data curation, Conceptualization. **Andreas Blennow:** Writing – review & editing, Conceptualization. **Ke Guo:** Writing – review & editing, Methodology. **Sheng Chen:** Writing – review & editing. **Liselotte Jauffred:** Writing – review & editing. **Poul Martin Bendix:** Writing – review & editing. **Jacob Judas Kain Kirkensgaard:** Methodology, Investigation. **Staffan Persson:** Writing – review & editing, Supervision, Resources, Funding acquisition, Conceptualization. **Yuyue Zhong:** Writing – review & editing, Writing – original draft, Supervision, Resources, Methodology, Investigation, Data curation, Conceptualization.

Declaration of competing interest

The authors declare that they have no known competing financial interests or personal relationships that could have appeared to influence the work reported in this paper.

Acknowledgements

Some imaging data were collected at the Center for Advanced Bioimaging (CAB) Denmark. This study was financially supported by grants from Jiangsu Funding Program for Excellent Postdoctoral Talent (2024ZB706, 2025ZB30), Jiangsu Province Young Science and Technology Talent Lifting Project (JSTJ-2024-328). X-ray scattering data was produced by a research infrastructure at the University of Copenhagen, partly funded by FOODHAY (Food and Health Open Innovation Laboratory, Danish Roadmap for Research Infrastructure). S.P. was funded by a Villum and three Novo Nordisk Foundation grants (25915, 19OC0056076, 20OC0060564, 23OC0086341, respectively).

Appendix A. Supplementary data

Supplementary data to this article can be found online at https://doi.org/10.1016/j.foodchem.2026.148970.

Data availability

No data was used for the research described in the article.

References

Abraham, Y., & Elbaum, R. (2013). Quantification of microfibril angle in secondary cell walls at subcellular resolution by means of polarized light microscopy. *New Phytologist, 197*(3), 1012–1019. https://doi.org/10.1111/nph.12070

Anand, A., Chhaniwal, V., & Javidi, B. (2018). Tutorial: Common path self-referencing digital holographic microscopy. *APL Photonics, 3*(7).

Ballard, Z. S., Zhang, Y., & Ozcan, A. (2017). Off-axis holography and micro-optics improve lab-on-a-chip imaging. *Light: Science & Applications, 6*(9), Article e17105.
Bertoft, E. (2017). *Understanding starch structure: Recent progress. Agronomy, 7*(3), 56.
Biliaderis, C. G., Page, C. M., Maurice, T. J., & Juliano, B. O. (1986). Thermal characterization of rice starches: A polymeric approach to phase transitions of granular starch. *Journal of Agricultural and Food Chemistry, 34*(1), 6–14.
Bunker, J. W., & Anderson, E. G. (1928). Polarized light and starch hydrolysis. *Journal of Biological Chemistry, 77*(2), 473–488.
Cai, C., Lin, L., Man, J., Zhao, L., Wang, Z., & Wei, C. (2014). Different structural properties of high-amylose maize starch fractions varying in granule size. *Journal of Agricultural and Food Chemistry, 62*(48), 11711–11721.
Cai, C., & Wei, C. (2013). In situ observation of crystallinity disruption patterns during starch gelatinization. *Carbohydrate Polymers, 92*(1), 469–478.
Cai, C., Zhao, L., Huang, J., Chen, Y., & Wei, C. (2014). Morphology, structure and gelatinization properties of heterogeneous starch granules from high-amylose maize. *Carbohydrate Polymers, 102*, 606–614.
Colomb, T., Dürr, F., Cuche, E., Marquet, P., Limberger, H. G., Salathé, R.-P., & Depeursinge, C. (2005). Polarization microscopy by use of digital holography: Application to optical-fiber birefringence measurements. *Applied Optics, 44*(21), 4461–4469.
Coppola, G., & Ferrara, M. A. (2020). Polarization-sensitive digital holographic imaging for characterization of microscopic samples: Recent advances and perspectives. *Applied Sciences, 10*(13), 4520.
Corgneau, M., Gaiani, C., Petit, J., Nikolova, Y., Banon, S., Ritié-Pertusa, L., … Scher, J. (2019). Digestibility of common native starches with reference to starch granule size, shape and surface features towards guidelines for starch-containing food products. *International Journal of Food Science & Technology, 54*(6), 2132–2140.
Dankar, I., Haddarah, A., Omar, F. E., Pujolà, M., & Sepulcre, F. (2018). Characterization of food additive-potato starch complexes by FTIR and X-ray diffraction. *Food Chemistry, 260*, 7–12.
Ding, L., Xie, Z., Fu, X., Wang, Z., Huang, Q., & Zhang, B. (2021). Structural and in vitro starch digestion properties of potato parenchyma cells: Effects of gelatinization degree. *Food Hydrocolloids, 113*, Article 106464.
Ebrahimi, S., & Dashtdar, M. (2021). Lens-free digital holographic microscopy for cell imaging and tracking by Fresnel diffraction from a phase discontinuity. *Optics Letters, 46*(15), 3516–3519.
Ebrahimi, S., Dashtdar, M., Fonda, C., & Cabrera, H. (2025). Field-portable digital holographic quantitative phase imaging with a compact microscope's add-on module. *Optics and Lasers in Engineering, 184*, Article 108580.
Ebrahimi, S., Dashtdar, M., Sánchez-Ortiga, E., Martínez-Corral, M., & Javidi, B. (2018). Stable and simple quantitative phase-contrast imaging by Fresnel biprism. *Applied Physics Letters, 112*(11).
Ebrahimi, S., Moreno-Pescador, G., Persson, S., Jauffred, L., & Bendix, P. M. (2023). Label-free optical interferometric microscopy to characterize morphodynamics in living plants. *Frontiers in Plant Science, 14*, Article 1156478.
Evers, A. (1971). Scanning electron microscopy of wheat starch. III. Granule development in the endosperm. *Starch-Stärke, 23*(5), 157–162.
Fuwa, H., Sugimoto, Y., Takaya, T., & Nikuni, Z. (1979). Scanning electron-microscopy of starch granules, with or without amylase attack. *Carbohydrate Research, 70*(2), 233–238.
Genkina, N. K., Kozlov, S. S., Martirosyan, V. V., & Kiseleva, V. I. (2014). Thermal behavior of maize starches with different amylose/amylopectin ratio studied by DSC analysis. *Starch-Stärke, 66*(7–8), 700–706.
Genyi, Z., Zihua, A., & Hamaker, B. R. (2006). Slow digestion property of native cereal starches. *Biomacromolecules, 7*(11), 3252.
Goodwin, G., Lim, D., Mahajan, S., & Nolte, D. D. (2025). Fresnel biprism common-path low-coherence digital holography for dynamic light scattering spectroscopy of biological materials. *Biomedical Optics Express, 16*(2), 806–820.
Guo, K., Tian, Y., Podzimska-Sroka, D., Kirkensgaard, J. J. K., Herburger, K., Enemark-Rasmussen, K., … Zhong, Y. (2024). Structural evolution of maize starches with different amylose content during pasting and gelation as evidenced by rapid Visco analyser. *Food Chemistry, 461*, Article 140817. https://doi.org/10.1016/j.foodchem.2024.140817
Han, X., Wen, H., Luo, Y., Yang, J., Xiao, W., Ji, X., & Xie, J. (2021). Effects of α-amylase and glucoamylase on the characterization and function of maize porous starches. *Food Hydrocolloids, 116*, Article 106661.
Hernández, J. M., Gaborieau, M., Castignolles, P., Gidley, M. J., Myers, A. M., & Gilbert, R. G. (2008). Mechanistic investigation of a starch-branching enzyme using hydrodynamic volume SEC analysis. *Biomacromolecules, 9*(3), 954–965.
Kemper, B., & Von Bally, G. (2008). Digital holographic microscopy for live cell applications and technical inspection. *Applied Optics, 47*(4), A52–A61.
Lim, J., Zhang, X., Ferruzzi, M. G., & Hamaker, B. R. (2019). Starch digested product analysis by HPAEC reveals structural specificity of flavonoids in the inhibition of mammalian α-amylase and α-glucosidases. *Food Chemistry, 288*, 413–421.
Liu, Q., Charlet, G., Yelle, S., & Arul, J. (2002). Phase transition in potato starch–water system I. Starch gelatinization at high moisture level. *Food Research International, 35*(4), 397–407.
Lourdin, D., Putaux, J.-L., Potocki-Véronèse, G., Chevigny, C., Rolland-Sabaté, A., & Buléon, A. (2015). Crystalline structure in starch. In Y. Nakamura (Ed.), *Starch: Metabolism and structure* (pp. 61–90). Tokyo: Springer Japan.
Mehta, S. B., Shribak, M., & Oldenbourg, R. (2013). Polarized light imaging of birefringence and diattenuation at high resolution and high sensitivity. *Journal of Optics, 15*(9), Article 094007.
Merola, F., Memmolo, P., Miccio, L., Bianco, V., Paturzo, M., & Ferraro, P. (2015). Diagnostic tools for lab-on-chip applications based on coherent imaging microscopy. *Proceedings of the IEEE, 103*(2), 192–204.
Muñoz, L. A., Pedreschi, F., Leiva, A., & Aguilera, J. M. (2015). Loss of birefringence and swelling behavior in native starch granules: Microstructural and thermal properties. *Journal of Food Engineering, 152*, 65–71. https://doi.org/10.1016/j.jfoodeng.2014.11.017
Nguyen, T. H., Kandel, M. E., Rubessa, M., Wheeler, M. B., & Popescu, G. (2017). Gradient light interference microscopy for 3D imaging of unlabeled specimens. *Nature Communications, 8*(1), 210. https://doi.org/10.1038/s41467-017-00190-7
Nikuni, Z. (1978). Studies on starch granules. *Starch-Stärke, 30*(4), 105–111.
Patel, B. K., & Seetharaman, K. (2006). Effect of heating rate on starch granule morphology and size. *Carbohydrate Polymers, 65*(3), 381–385.
Pérez, S., Baldwin, P. M., & Gallant, D. J. (2009). Structural features of starch granules I. In *Starch* (pp. 149–192). Elsevier.
Pérez, S., & Bertoft, E. (2010). The molecular structures of starch components and their contribution to the architecture of starch granules: A comprehensive review. *Starch-Stärke, 62*(8), 389–420. https://doi.org/10.1002/star.201000013
Ratnayake, W. S., & Jackson, D. S. (2008). Starch gelatinization. *Advances in Food and Nutrition Research, 55*, 221–268.
Shrestha, A. K., Jaroslav, B., Flanagan, B. M., Sushil, D., Oscar, L., Morell, M. K., … Gidley, M. J. (2012). Molecular, mesoscopic and microscopic structure evolution during amylase digestion of maize starch granules. *Carbohydrate Polymers, 90*(1), 23–33.
Tian, Y., Petersen, B. L., Liu, X., Li, H., Kirkensgaard, J. J. K., Enemark-Rasmussen, K., … Blennow, A. (2024). Characterization of different high amylose starch granules. Part II: Structure evolution during digestion and distinct digestion mechanisms. *Food Hydrocolloids, 149*, Article 109593.
Tian, Y., Wang, Y., Liu, X., Herburger, K., Westh, P., Møller, M. S., … Blennow, A. (2023). Interfacial enzyme kinetics reveals degradation mechanisms behind resistant starch. *Food Hydrocolloids, 140*, Article 108621.
Tsai, C.-M., Vyas, S., & Luo, Y. (2024). Common-path digital holographic microscopy based on a volume holographic grating for quantitative phase imaging. *Optics Express, 32*(5), 7919–7930.
Wang, S., & Copeland, L. (2015). Effect of acid hydrolysis on starch structure and functionality: A review. *Critical Reviews in Food Science and Nutrition, 55*(8), 1081–1097.
Warren, F. J., Gidley, M. J., & Flanagan, B. M. (2016). Infrared spectroscopy as a tool to characterise starch ordered structure—A joint FTIR–ATR, NMR, XRD and DSC study. *Carbohydrate Polymers, 139*, 35–42.
Wei, C., Zhang, J., Chen, Y., Zhou, W., Xu, B., Wang, Y., & Chen, J. (2010). Physicochemical properties and development of wheat large and small starch granules during endosperm development. *Acta Physiologiae Plantarum, 32*, 905–916.
Xiao, H., Wang, S., Xu, W., Yin, Y., Xu, D., Zhang, L., … Lin, Q. (2020). The study on starch granules by using darkfield and polarized light microscopy. *Journal of Food Composition and Analysis, 92*, Article 103576.
Yaghoubi, S. H. S., Ebrahimi, S., & Dashtdar, M. (2022). Structured illumination in Fresnel biprism-based digital holographic microscopy. *Optics and Lasers in Engineering, 159*, Article 107215. https://doi.org/10.1016/j.optlaseng.2022.107215
Yang, Z., Gu, Q., & Hemar, Y. (2013). In situ study of maize starch gelatinization under ultra-high hydrostatic pressure using X-ray diffraction. *Carbohydrate Polymers, 97*(1), 235–238.
Yeh, A.-I., & Li, J.-Y. (1996). A continuous measurement of swelling of rice starch during heating. *Journal of Cereal Science, 23*(3), 277–283.
Zhong, Y., Bertoft, E., Li, Z., Blennow, A., & Liu, X. (2020). Amylopectin starch granule lamellar structure as deduced from unit chain length data. *Food Hydrocolloids, 108*, Article 106053.
Zhong, Y., Liu, L., Qu, J., Blennow, A., Hansen, A. R., Wu, Y., … Liu, X. (2020). Amylose content and specific fine structures affect lamellar structure and digestibility of maize starches. *Food Hydrocolloids, 108*, Article 105994.
Zhong, Y., Qu, J. Z., Liu, X., Ding, L., Liu, Y., Bertoft, E., … Blennow, A. (2022). Different genetic strategies to generate high amylose starch mutants by engineering the starch biosynthetic pathways. *Carbohydrate Polymers, 287*, Article 119327.